Available online at www.sciencedirect.com
ScienceDirect
Precambrian Research 149 (2006) 231–248
Precambrian Research
www.elsevier.com/locate/precamres

Isotope stratigraphy of the Lapa Formation, São Francisco Basin, Brazil: Implications for Late Neoproterozoic glacial events in South America

Karem Azmy [a,*], Alan J. Kaufman [b], Aroldo Misi [c], Tolentino Flávio de Oliveira [d]

[a] Department of Earth Sciences, Memorial University of Newfoundland, St. John's, Nfld A1B 3X5, Canada
[b] Geology Department, University of Maryland, College Park, MD 20742, USA
[c] Centro de Pesquisa em Geofisica e Geologia e Curso de Pós-Graduação em Geologia, Instituto de Geociências/CPGG, Universidade Federal da Bahia, Salvador, Bahia 40210-340, Brazil
[d] Votorantim Metais, P.O. Box 03, 38780-000 Vazante MG, Brazil

Received 9 March 2006; received in revised form 28 June 2006; accepted 6 July 2006

Abstract

The Lapa Formation is a thick carbonate sequence (∼900 m) that constitutes the upper part of the Vazante Group on the São Francisco craton, Brazil. It conformably overlies a previously unrecognized glacial diamictite unit of poorly constrained age. The sequence, above the glacial unconformity, consists predominantly of organic-rich shale, subtidal rhythmic dolomicrites and microbialaminites, and intertidal stromatolites. Four boreholes, spanning different depositional settings, were sampled at high-resolution and investigated for their petrographic and chemical criteria to evaluate their degree of preservation.

The $\delta^{13}C$ and $\delta^{18}O$ values of well preserved Lapa carbonate microsamples range from −8.2‰ to 3.3‰ (VPDB) and from −13.6‰ to −0.9‰ (VPDB), respectively. Each of the $\delta^{13}C$ profiles of the investigated cores reveals two strong negative excursions of up to 8‰, an event in post-glacial dolomicrites immediately above the glaciogenic unit and a 10 m interval of organic-rich shale, and a second near the top of the sequence associated with a shale interval. Based on the observation of dropstones and sedimentary iron formation in the underlying diamictite, as well as the distinguishable carbon isotope trends, the Lapa Formation is considered as a cap carbonate lithofacies. The age of the Lapa Formation is presently unknown but the least radiogenic $^{87}Sr/^{86}Sr$ value (∼0.7068), associated with a negative carbon isotope excursion, matches that from the Rasthof Formation in Namiba on the Congo craton, which is radiometrically constrained to be younger than ca. 750 Ma.

Keywords: Neoproterozoic carbonates; Stable isotope stratigraphy; Lapa Formation; Brazil

1. Introduction

The successful use of stable isotope signatures encrypted in Phanerozoic marine carbonates (cf. Veizer et al., 1999 and references therein) to understand Earth's surface evolution encouraged Neoproterozoic (1000–543 Ma) researchers to apply these same techniques to the investigation of changing surface environments and life on Earth. Lacking a biostratigraphic framework and a dearth of radiometric dates in most basins, chemostratigraphy has thus become the hallmark of Proterozoic correlation (e.g., Knoll et al., 1986; Kaufman and Knoll, 1995; Shields et al., 1998; Jacobsen and Kaufman, 1999; Brasier and Shields, 2000; Azmy

* Corresponding author. Tel.: +1 709 737 6731; fax: +1 709 737 2589.
E-mail address: kazmy@mun.ca (K. Azmy).

0301-9268/$ – see front matter © 2006 Elsevier B.V. All rights reserved.
doi:10.1016/j.precamres.2006.07.001

et al., 2001; Shields and Veizer, 2002; Cozzi et al., 2004). This is especially so in the thick Neoproterozoic successions of Brazil, including the carbonate-dominated Vazante Group (Azmy et al., 2001) and their equivalents on the São Francisco craton. During the Neoproterozoic, this craton was a conjugate to the Congo craton in Africa, which includes the glaciogenic Otavi Group where the 'Snowball Earth' hypothesis was resurrected (Kirschvink, 1992; Hoffman et al., 1998a).

Ongoing chemostratigraphic investigations in Brazil aim to refine regional and global correlations of glacial diamictites at the base of the Vazante and Bambuí groups, in order to better understand the evolution of surface environments and climate near the end of the Proterozoic Eon. In this study, we investigate the upper reaches of the Vazante Group, including the Morro do Calcario Formation and the overlying Lapa Formation for evidence of glacial phenomenon and associated stable isotope anomalies. Using these observations, we predict correlations with better dated units on the Congo Craton and thus provide chemostratigraphic constraints on the co-evolution of both successions.

2. Geologic setting

The Lapa Formation is a part of the carbonate-dominated Neoproterozoic platform of the Vazante Group (Dardenne, 2001) that extends along more than 300 km N–S in the external zone of the Brasilia Fold Belt in São Francisco Basin (Fig. 1). The stratigraphy of the marginal marine sediments of the Vazante Group (Fig. 2) has been studied in detail and refined by several authors (e.g., Dardenne, 1978; Dardenne and Walde, 1979; Madalosso, 1979; Karfunkel and Hoppe, 1988; Fairchild et al., 1996; Azmy et al., 2001; Dardenne, 2001; Misi, 2001; Misi et al., in press). In the eastern part of the basin, carbonate, diamictite, and shale of the Vazante Group are generally well preserved and little metamorphosed; to the west near the Brazilia Fold

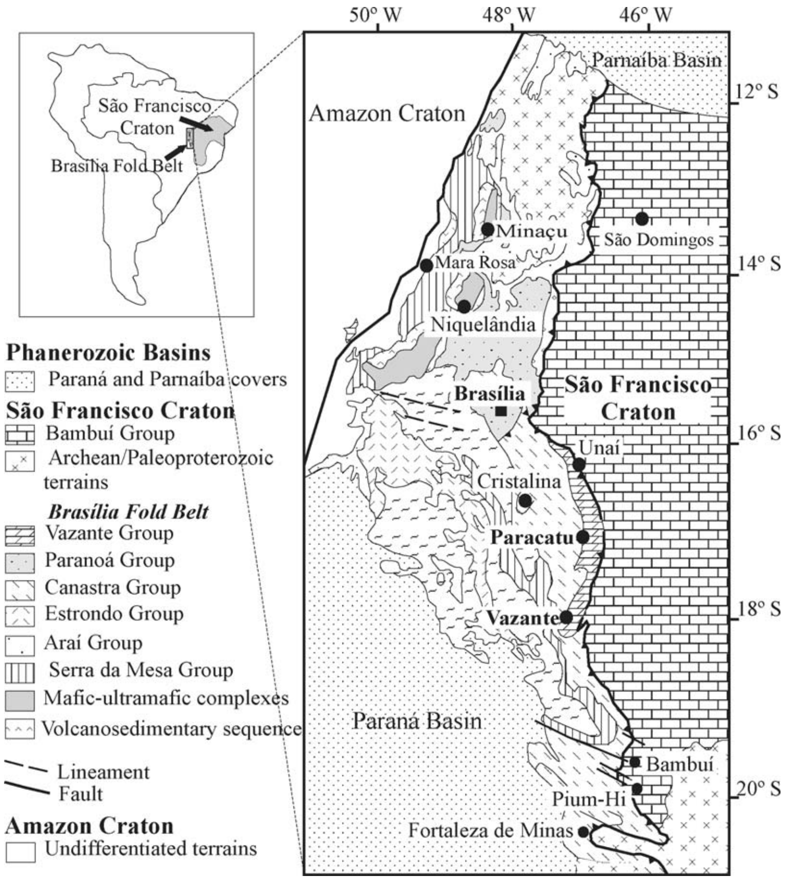

Fig. 1. Location map of São Francisco Basin in Brazil showing the geology of the Brasilia Fold Belt including the Vazante Group (modified from Valeriano et al., 2004).

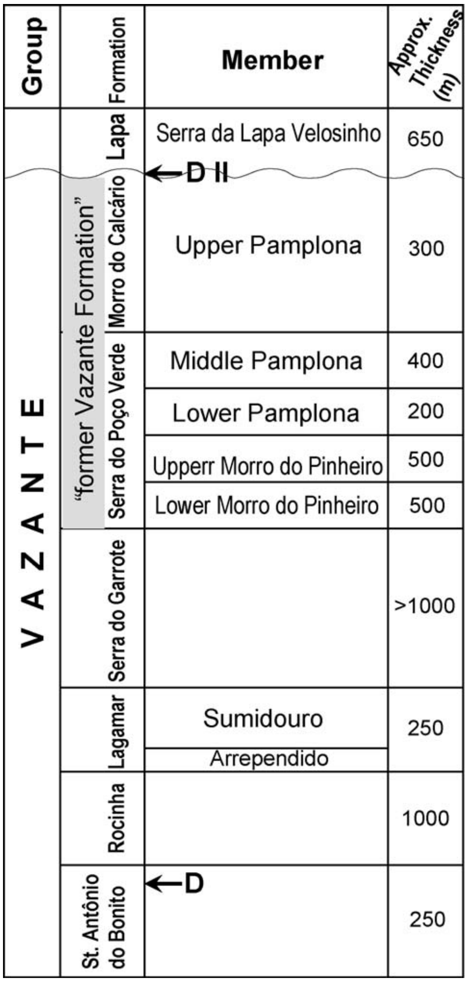

Fig. 2. A schematic diagram of Vazante Group stratigraphy showing the levels of the glacial intervals (D) at the top of Santo Antônio do Bonito Formation and DII at the base of Lapa Formation (modified from Dardenne, 2001).

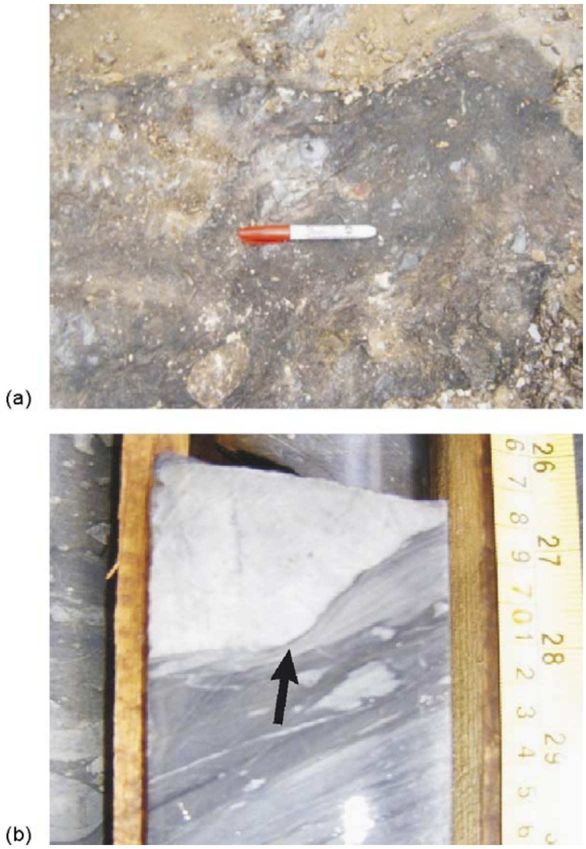

Fig. 3. Photographs of (a) lower diamictite unit (D) at the top of San Antonio do Bonito Formation and (b) a core slab from the uppermost diamictite unit (DII) at the base of Lapa Formation, the arrow points at a dropstone.

Belt, however, the sediments are highly deformed and have experienced amphibolite to granulite facies metamorphism. (Dardenne, 1978; Fuck et al., 1994). While earlier investigations indicated that the Vazante Group sediments accumulated in a passive margin setting (e.g., Campos-Neto, 1984; Fuck et al., 1994), recent studies suggest that these sediments were deposited in a foreland basin during the initial phases of the Brasiliano orogeny (e.g., Dardenne, 2000).

The Vazante Group is believed to have a basal glaciogenic unit (D), which constitutes the uppermost part of the Santo Antônio do Bonito Formation (Figs. 2 and 3a) and has also been broadly correlated with glacial strata that form the base of the Bambuí Group to the east (Dardenne, 2001; Misi et al., in press). However, new observations of carbonate breccia and dropstones in interbedded organic-rich shale (Figs. 2 and 3b) in overlying horizons indicate the presence of a second glacial horizon (DII) near the top of the Vazante succession (Olcott et al., 2005) immediately beneath the Lapa Formation. Sedimentary iron-formation and iron oxide cemented diamictites are also noted near the top of this second glaciogenic interval (Brody et al., 2004). A regional unconformity (Fig. 2) is believed to have occurred at the base of the upper diamictite (DII) throughout the entire basin (Misi et al., 2005).

The Lapa Formation, which overlies the younger diamictites (DII), is predominantly composed of rhythmically laminated argillaceous dolomites (Fig. 4a), with shales in the upper part. Immediately above the upper Vazante Group diamictite (DII), Lapa sediments begin with a ca. 10 m thick organic rich shale that contains outsized clasts of underlying carbonate lithologies, which truncate the finely laminated sediment and are inter-

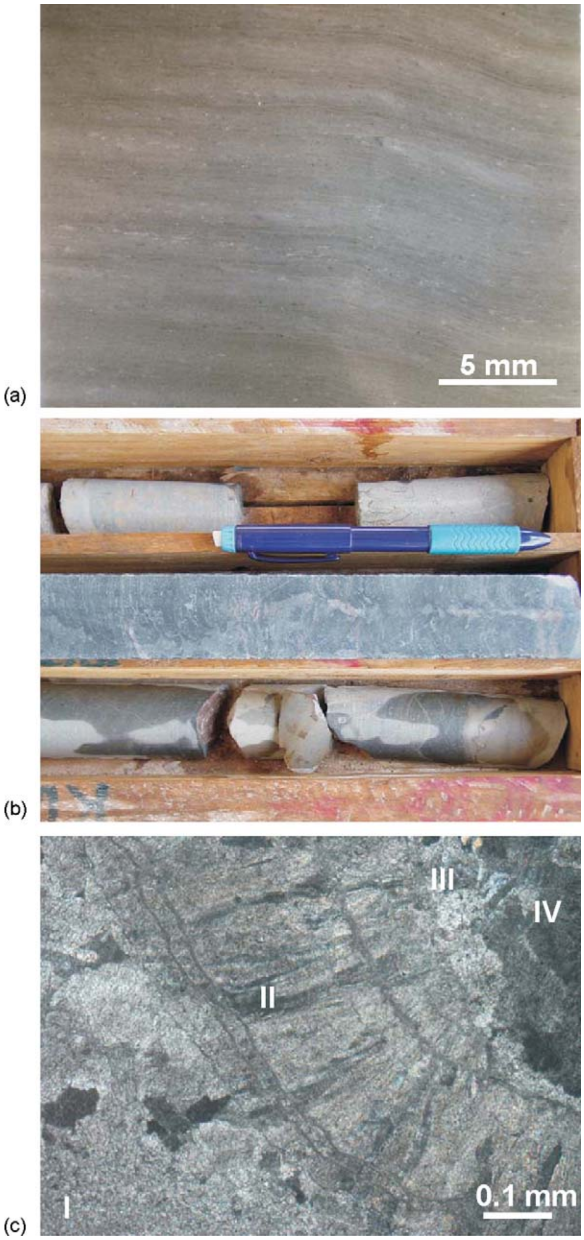

Fig. 4. Images from Lapa Formation carbonates showing main petrographic features: (a) photograph of a polished slab (Sample F 19) showing rhythmites from subtidal facies of Core MAF 38-84, (b) photograph of stromatolites in a slab of Core KVD-F60 at a depth of 602 m, and (c) photomicrograph of a thin section (sample KVD 60-16) under crossed Nichols with dolomite generations (I–IV) identical to those described by Azmy et al. (2001) in the underlying Pamplona carbonates.

preted as dropstones (Fig. 3b) deposited during post-glacial transgression (Brody et al., 2004). The Lapa sediments vary from intertidal dolomitized lime mudstone with stromatolitic lenses (Azmy et al., 2001) to subtidal laminated dolomitized lime mudstone alternating with clays or shales, forming rhythmites (Fig. 4a). Shallowing of the basin into the photic zone resulted in the formation of occasional stromatolites (Fig. 4b) above the shale, but most of the overlying succession consists of thick rhythmically bedded argillaceous dolomite and microbialaminite.

Petrographic examination of thin sections shows that the dolomicrites are notably very fine grained (Fig. 4c) and are generally fabric retentive. Three generations of secondary dolomitic cements have been observed; including fibrous, equant, and late fracture-filling phases (cf. Azmy et al., 2001). No significant increase in crystal size was observed associated with dolomitization of the lime mud precursors, suggesting that the original sediment did not suffer from extensive and/or repeated meteoric alteration.

3. Radiometric age constraints

The age of the Vazante Group and Lapa Formation are poorly constrained. No volcanic ash layers have yet been discovered, which argue against the foreland basin depositional model suggested recently by some authors. Based on the occurrence of *Conophyton metula Kirichenko* in the Lagamar Formation (Fig. 2), Cloud and Dardenne (1973) suggested an age of between 1350 and 950 Ma for the lower Vazante Group. Radiometric constraints based on whole rock Rb/Sr or Pb/Pb determinations are problematic and likely represent overprinted ages due to the effects of the Braziliano Orogeny (Lagoeiro, 1990; Alkmim et al., 1993; Chemale et al., 1993; D'Agrella-Fihlo et al., 2000; Misi et al., in press and more references therein).

4. Methodology

Four parallel cores (separated laterally by as much as 45 km), provided by the Brazilian mining company Votorantim Metais, which intersected the Lapa Formation and the underlying glacial diamictite (Figs. 2 and 3b) were investigated and sampled at high resolution (Appendix A). These cores included: MASW 01 (17°31′58″S/46°51′09″W), PMA 04 (17°29′32″S/46°49′23″W), MAF 38-84 (17°29′46″S/46°49′46″W), and KVD-F60 (17°46′34″S/46°47′02″W); these drillholes were carefully selected to avoid tectonic complications. The sedimentary layers in the studied cores are nearly horizontal, with few exceptions, and their thicknesses have not been corrected.

Thin sections of the samples were examined petrographically with a polarizing microscope and cathodoluminoscope and stained with Alizarin Red-S and potassium ferricyanide solutions (Dickson, 1966). A mirror-image slab of each thin section was also prepared and polished for microsampling. Cathodoluminescence observations were performed using a Technosyn 8200 MKII cold cathode instrument operated at ∼11 kV accelerating voltage and ∼450 mA current intensity. Some selected samples were analyzed by XRD to further refine mineralogic compositions and some bulk powder samples were acidified in microcentrifuge tubes and then dried to determine the percent of carbonate in representative lithologies throughout the Lapa Formation.

Polished slabs were washed with deionized water and dried overnight at 50 °C prior to the isolation of the finest grained dolomicrites free of secondary cements. Approximately, 4 mg were microsampled from the cleaned slabs with a low-speed microdrill. The geochemical analyses have been mainly run on the microsampled powder except for those of the evaluation of carbonate contents and the measurements of $\delta^{13}C$ of organic carbon that were run on bulk sample powders. For C- and O-isotope analyses, about 500 μg of powder sample was reacted in inert atmosphere with ultrapure concentrated (100%) orthophosphoric acid at 72 °C in a ThermoFinnigan Gasbench II. The headspace CO_2 produced from the reaction was automatically flushed through a chromatographic column and delivered to the source of a ThermoFinnigan DELTA plus XP isotope ratio mass spectrometer in a stream of helium, where the gas was ionized and measured for isotope ratios. Uncertainties of better than 0.1‰ (2σ) for the analyses were determined by repeated measurements of NBS-19 ($\delta^{18}O = -2.20$‰ and $\delta^{13}C = +1.95$‰ versus V-PDB) and NBS-18 ($\delta^{18}O = -3.00$‰ and $\delta^{13}C = -5.00$‰ versus V-PDB) standards during each run of samples.

For elemental analyses, a subset of sample powder was digested in 5% (v/v) acetic acid for 70–80 min. and analysed for Ca, Mg, Sr, and Mn (Coleman et al., 1989) using a HP 4500^{plus} at Memorial University of Newfoundland. The relative uncertainties of these measurements are better than 5%.

Organic carbon isotope ratios were measured on isolated kerogen after repeated treatment with concentrated hydrochloric acid at the isotope laboratory of Memorial University of Newfoundland, using a Carlo Erba Elemental Analyzer coupled to a 252 Finnigan Mat Mass Spectrometer. The results were normalized to the standards IAEA-CH-6 ($\delta^{13}C = -10.43$), NBS18 ($\delta^{13}C = -5.04$) and USGS24 ($\delta^{13}C = -15.99$) and the uncertainty calculated from repeated measurements was ∼0.2‰.

Guided by petrographic observations, some samples were chosen for Sr-isotope analysis. About 2 mg of the powdered sample was dissolved in 2.5N ultrapure HCl and, after evaporation, Sr was extracted with quartz glass ion exchange columns filled with Bio Rad AG50WX8 resin. Finally, ∼75–100 ng Sr was loaded on Re filaments using a Ta2O5–HNO3–HF–H3PO4 solution. Measurements were performed with a Finnigan MAT 262 multicollector mass spectrometer at the Institut für Geologie, Mineralogie und Geophysik, Ruhr Universität, Bochum, Germany (cf. Diener et al., 1996; Azmy et al., 1999). Two standard reference materials were utilized as quality control of Sr isotope ratio measurements, NIST (NBS) 987 and USGS EN–1, which gave mean $^{87}Sr/^{86}Sr$ values over the analyses interval of 0.710236 ± 0.0000008 and 0.709151 ± 0.000008, respectively.

Trace sulfate in carbonate was isolated following the method outlined by Hall et al. (1988), at the Environmental Isotope Laboratory of the University of Waterloo, Ontario, Canada. Resulting barites were measured for their sulfur isotope compositions by continuous flow techniques using a Carlo Erba Elemental Analyser (CHNS-O) EA 1108 in line with a Micromass Isoprime mass spectrometer. Results are reported in the standard δ notation relative to the Canyon Diablo Triolite standard (V-CDT) with 1σ precisions of better than ±0.3‰ based on multiple analyses of standard materials during the run of samples.

5. Results and discussion

The primary concern of this study is whether the negative $\delta^{13}C$ excursions in carbonates from argillaceous lithofacies at the base and near the top of the Lapa Formation reflect environmental or diagenetic perturbations (Appendix A). If primary, these biogeochemical anomalies may be considered in the context of widespread Neoproterozoic ice ages and be compared with similar events on other continents. Therefore, the evaluation of the encrypted geochemical signatures in the Lapa carbonates is a cornerstone for the reconstructions of reliable chemostratigraphic profiles.

5.1. Evaluation of sample preservation

Several petrographic and geochemical screens have been utilized to ascertain the degree of preservation of carbonate-rich laminae in samples of the Lapa carbonates (e.g., Kaufman et al., 1991, 1992, 1993; Derry et al., 1992; Narbonne et al., 1994; Misi and Veizer, 1998; Azmy et al., 2001). Thin sections were examined using a petrographic microscope for grain size, degree of recrystallization, detrital and organic matter contents and sedimentary structures. In general, we find that carbonates in these argillaceous sediments are not significantly recrystallized and retain primary sedimentary fabrics. Cathodoluminescence (CL) was also employed to study the different rock components and to refine the selection of best preserved carbonates (e.g., Azmy et al., 2001). Notably, luminescence in carbonates is mainly activated by high concentrations of Mn and quenched by high concentrations of Fe (Machel and Burton, 1991). High degrees of luminescence, in many cases, indicates diagenetic alteration by meteoric water but this interpretation should be taken with caution insofar as some altered carbonates might exhibit no luminescence due to high Fe contents (Rush and Chafetz, 1990), and some primary carbonates (especially those deposited during Neoproterozoic post-glacial transgression) might be enriched in both Fe and Mn due to widespread ocean anoxia during ice ages (Corsetti and Kaufman, 2003).

Due to the possible heterogeneity in geochemical composition of texturally distinct carbonate phases in whole-rock samples, and in order to avoid silicate-rich intervals, secondary cement and veins, microsamples were drilled from the finest grained and purest carbonate phases. Microsamples were then analyzed for their elemental and isotopic compositions. Of particular interest are the Mn and Sr abundances and oxygen isotope compositions of microsamples as these can be readily redistributed by alteration under the influence of meteoric fluids (Brand and Veizer, 1980; Veizer, 1983).

The Mn/Sr ratio of marine carbonates has been utilized as a tool for screening samples and evaluating their degree of preservation in Neoproterozoic successions (e.g., Derry et al., 1992; Kaufman and Knoll, 1995). However, studies from different basins have come to significantly different conclusions as to the cutoff ratio for "well preserved" versus "altered" samples with respect to either C or Sr isotope compositions. In general, lower ratios (indicating higher Sr concentrations) are preferred for the Sr isotope studies, while higher ratios (up to 10) have been accepted for C isotope studies, in large part due to the buffering effect of carbonate carbon relative to the bicarbonate abundance of diagenetic solutions (Kaufman and Knoll, 1995; Corsetti and Kaufman, 2003). The Mn/Sr in drilled Lapa dolomicrites range from near 0 to 10, except for very few cases that reach up to 15, with Sr concentrations reaching up to ~500 ppm (Appendix A). Insofar as dolomitization would tend to drive Sr from carbonates, it is not unexpected to find higher Mn/Sr in these pervasively dolomitized sediments. Based on these measurements alone it is unlikely

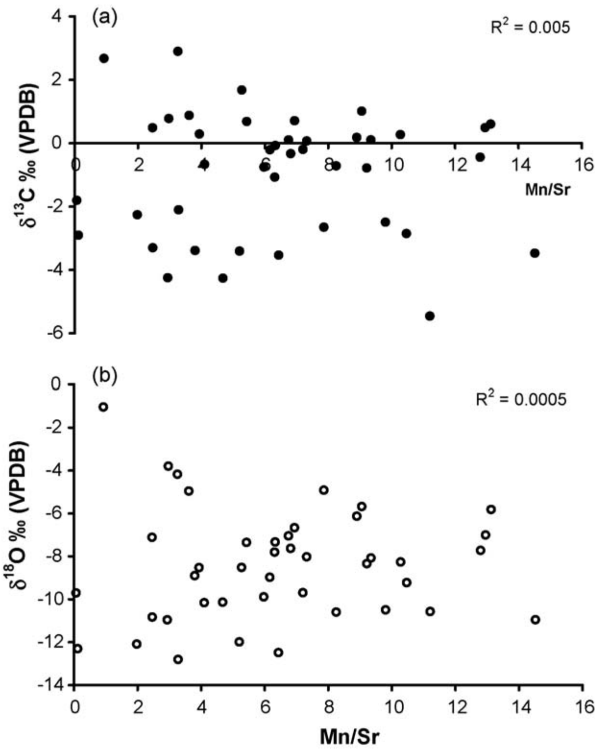

Fig. 5. A scatter diagram of Mn/Sr vs. (a) $\delta^{13}C$ and (b) $\delta^{18}O$ for dolomicrites (carbonate mud) of the Lapa Formation.

that primary Sr isotope compositions would be preserved in this unit, baring exceptional cases. However, carbon isotopes of most samples may be considered as little altered given the lack of relationship between $\delta^{13}C$ and Mn/Sr values (Fig. 5a).

Oxygen isotope compositions of carbonates may also be sensitive monitors of diagenetic alteration by meteoric and metamorphic fluids, which are typically depleted in the heavy isotope relative to seawater solutions. The $\delta^{18}O$ signature of dolomites is generally influenced by that of the fluid because dolomitization requires large volumes of water to supply adequate Mg for the newly formed mineral. It is noteworthy, however, that dolomitization of the Lapa carbonates did not result in significant recrystallization and that sedimentary fabrics are largely retained. The Lapa dolomicrites, not including the secondary cements, have $\delta^{18}O$ values that range widely from −13.6 to −1.0‰ VPDB (Figs. 5b and 6), suggesting variable degrees of alteration. However, there is no systematic relationship between $\delta^{18}O$ (or $\delta^{13}C$) and Mn/Sr (Fig. 5b) values in this sample set. The lack of petrographic evidence for significant re-crystallization (cf. Banner and Hanson, 1990), the absence of any relationship between ^{13}C depletion and higher Mn/Sr, and

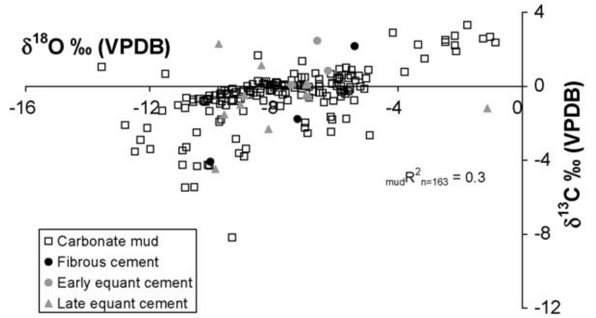

Fig. 6. Oxygen vs. carbon isotope values for the Lapa dolomite generations.

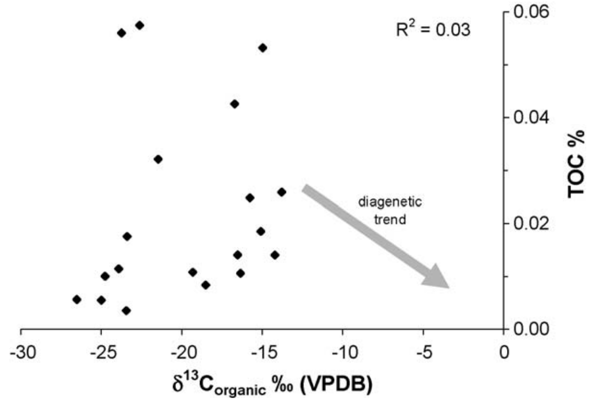

Fig. 8. A scatter diagram of δ^{13}C vs. the total organic carbon contents (TOC) the Lapa dolomicrites.

the consistency of values in closely spaced stratigraphic samples support the view that the strongly-to-moderately negative δ^{13}C compositions in the Lapa Formation dolomicrites reflect depositional conditions (cf. Knoll et al., 1986; Fairchild and Spiro, 1987; Burdett et al., 1990; Kaufman et al., 1991; Kaufman and Knoll, 1995; Jacobsen and Kaufman, 1999; Azmy et al., 2001).

Organic matter isolated from selected samples in a single core (Fig. 7) preserved a wide range of carbon isotope compositions, ranging from ca. −14 to −26‰. While the ^{13}C enrichment of some samples might be interpreted as a metamorphic artifact (Hayes et al., 1983), there appears to be no systematic relationship between carbon isotope enrichment and organic carbon abundance (Fig. 8) in the Lapa carbonates, which is also consistent with the estimated relative color differences of powdered bulk rock. Notably, the more siliciclastic- and organic-rich carbonates that typify the intervals at the base and top of the formation have significantly lower magnitudes of difference between organic and inorganic phases (reflected in $\Delta\delta$ values <20‰; Appendix A). In few (but not all) cases, the lower $\Delta\delta$ values are related to both ^{13}C depletion in carbonates and ^{13}C enrichment in the co-existing organic fraction. However, based on the mineralogy and fine textural preservation of the sediments there is no indication for large scale carbon isotope exchange in this system, and we interpret the variable $\Delta\delta$ trends as environmental, rather than diagenetic, artifacts. If correct, the ^{13}C enrichment of organic matter may reflect carbon limitation associated with extreme growth rates of primary producers in depositional settings (Kaufman et al., in press).

While the occurrrance of siliciclastic-rich lithofacies in the Lapa Formation makes chemostratigraphic

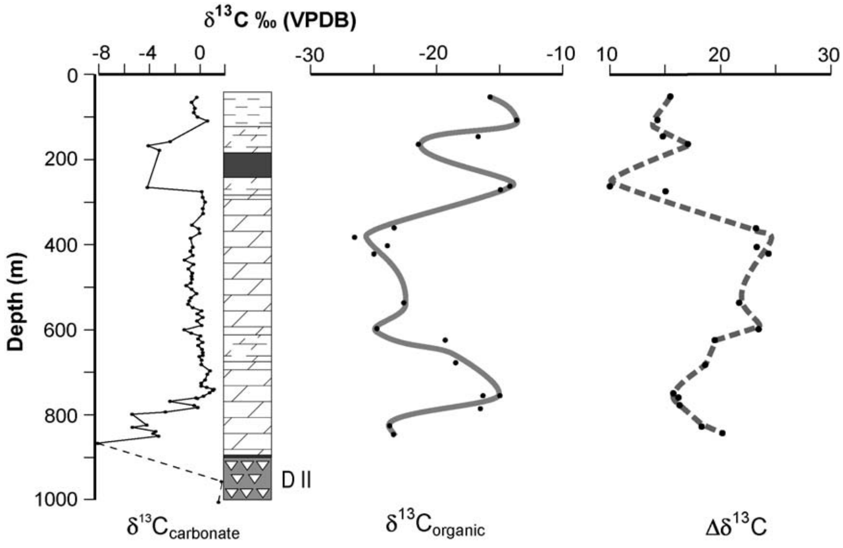

Fig. 7. A diagram showing the $\delta^{13}C_{carbonate}$, $\delta^{13}C_{organic}$ and $\Delta\delta$ profiles of the Lapa carbonates through the studied core MASW01. Legend as in Fig. 10.

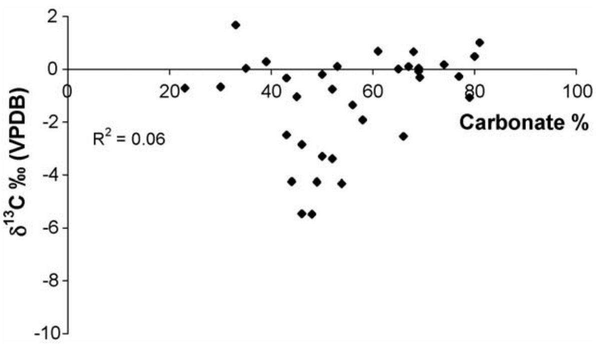

Fig. 9. The $\delta^{13}C$ values of Lapa dolomicrites vs. their carbonate contents.

analysis of ^{13}C variations in carbonates problematic, there is no clear relationship between carbonate abundance in bulk samples and ^{13}C depletion (Fig. 9). Intervals defined by strong negative $\delta^{13}C$ excursions contain similar carbonate abundances to those reflecting no isotope depletion. Furthermore, the consistency of $\delta^{13}C$ values in closely spaced stratigraphic samples support the view that the strongly-to-moderately negative $\delta^{13}C$ compositions in the Lapa Formation dolomicrites reflect depositional conditions (cf. Knoll et al., 1986; Fairchild and Spiro, 1987; Burdett et al., 1990; Kaufman et al., 1991; Kaufman and Knoll, 1995; Jacobsen and Kaufman, 1999; Azmy et al., 2001).

5.2. Isotope stratigraphy

Accepting that depositional $\delta^{13}C$ compositions of Lapa dolomicrites are preserved, or nearly so, we constructed stratigraphic profiles to investigate temporal variations in seawater chemistry at the time of deposition (Fig. 10). The $\delta^{13}C$ profiles of the Lapa Formation reveal variable expression of the basal negative carbon isotope anomaly in three of the cores (MASW01, PMA04, and MAF 38-84), and the upper anomaly also in three cores (MASW01, PMA04, and KVD-F60) assuming the latter section (KVD-F60) lacking basal diamictites captures only the upper portion of the Lapa Formation (Fig. 10).

At the base of the Lapa Formation directly above diamictites in laminated argillaceous dolomites, a negative $\delta^{13}C$ values as low as −8‰ is recorded in one core (other samples somewhat richer in carbonate have values nearer to −5‰); the other two cores house basal anomalies only as low as ca. −3‰. The variability between cores that are maximally separated by ~6 km may be the result of facies variations, stratal hiatus, diagenetic alteration in the argillaceous carbonates (Kaufman et al., in press), or possibly the degree of mixing of surface water with the ^{12}C-rich bottom water (e.g., Calver, 2000). The upper negative anomaly is associated with rhythmite facies, and is also variably expressed in the three cores ranging from −5 to around −3‰. The upper

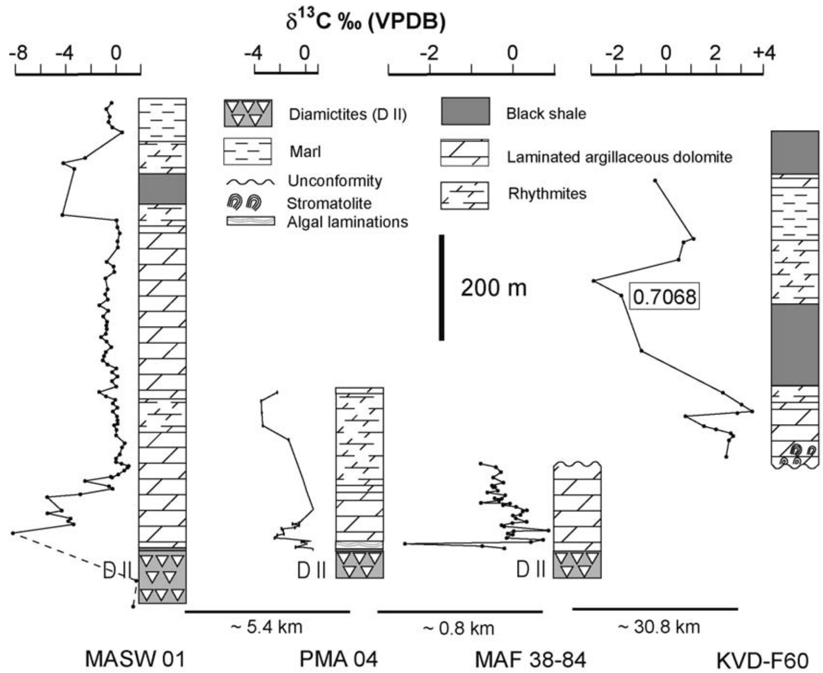

Fig. 10. The $\delta^{13}C$ profile of Lapa Formation showing consistent basinwide negative shifts in the four studied cores.

shift is missing in the profile of Core MAF 38-84, likely due to unconformity at the top of this section.

Specific tests of carbonate percentage (%) in MASW01 drillhole samples (Fig. 9) showed that the negative excursions are associated with samples containing 50% or less, carbonate. However, some samples within the interval of carbon isotope invariance contain even less carbonate, so there appears to be no direct correlation of abundance with isotope composition in the Lapa Formation. It is also noteworthy that significant reductions in $\Delta\delta$ seen at the level of the carbon isotope anomalies reflect both ^{13}C depletion in carbonate and ^{13}C enrichment in organic matter (Fig. 7). Since the stratigraphically restricted carbon isotope excursions are unlikely an outcome of regional metamorphism, we interpret the carbon isotope events at the base and top of the Lapa Formation as resulting from environmental perturbations in the depositional environment.

The basal biogeochemical event occurs in sediments directly above a glacial diamictite with dropstones in shaley lithofacies (Fig. 3b), and local expression of sedimentary iron formation, both of which are characteristic of Neoproterozoic glacial deposits. Hence, we interpret the basal Lapa succession as a "cap carbonate" lithofacies. There is no lithologic evidence for diamictite or other glacial phenomenon beneath the upper Lapa anomaly and its origin remains unknown, and therefore warrants further investigation. The organic-rich shale associated with the upper Lapa anomaly is a potential target for biomarker investigations (e.g., Brody et al., 2004; Olcott et al., 2005) and Re/Os radiometric measurements (e.g., Kendall et al., 2004) that may provide some clues on the timing and global correlation of the Neoproterozoic glaciations.

5.3. Correlation of the Lapa Formation

Recognition of the basal Lapa Formation as a Neoproterozoic cap carbonate lithofacies with a strong negative $\delta^{13}C$ anomaly provides possible clues to its age. Broadly speaking Neoproterozoic successions are thought to contain up to three discrete glacial horizons, classified as the Gaskiers, Marinoan (Varanger), and Sturtian events and radiometrically constrained to have occurred at ∼585 Ma (Bowring et al., 2003; Halverson et al., 2005), ∼630 Ma (Condon et al., 2005), and ∼750 Ma (Hoffman et al., 1996), respectively. Each of these has been shown to have strong carbon isotope anomalies, often in unusually textured carbonates immediately above the glacial deposits. Thus, correlation of the Lapa Formation to one of these events would provide indirect radiometric constraints on the Brazilian deposit. Because of the close association of the São Francisco and Congo cratons in Neoproterozoic time, a comparison with events in the Otavi and Witvlei groups is considered.

The Otavi Group contains two known diamictite/cap carbonate couplets, known as the Chuos/Rasthof and Ghaub/Maieberg (Hoffman et al., 1998a, 1998b). The lower cap is characterized by black (relatively organic rich) microbialaminite, stromatolite, and finely laminated ribbon rock. It has a carbon isotope anomaly that is also variably expressed, but generally has values down to −5‰, which trend to positive values over a short stratigraphic interval. Strontium isotope compositions of best preserved limestone from the Rasthof are as low as 0.7068 (Yoshioka et al., 2003; Halverson et al., 2005). In contrast, the celebrated Maieberg cap carbonate is composed of organic-poor stromatolitic (tubestone) and massive dolomicrite beds at the base overlain by deeper water limestone rhythmites with remarkable seafloor cements. Shallowing above this level is recognized by sedimentary fabrics and a progressive increase of dolomicrite. The carbon isotope anomaly in the Maieberg also falls to a nadir of ca. −5‰ in most sections, but negative values in this cap continue in some cases for up to 450 m. The limestone rhythmites with seafloor cements appear to be well preserved and have $^{87}Sr/^{86}Sr$ compositions of ca. 0.7073 (cf. Halverson et al., 2005). This value is an exact match for remarkably similar precipitates in a post-glacial cap from the nearby Bambuí Group (Fig. 1) in Brazil (cf. Misi and Veizer, 1998; Misi et al., in press).

In the Witvlei Group on the Kalahari Craton, there are also two recognized levels of glacial diamictite and cap carbonate (Kaufman et al., 1991, 1997a,b; Saylor et al., 1998). These are represented by the Blaubekker/Court and the Blazkranz/Tsabisis couplets and their regional equivalents. Like the Otavi Group, the lower limestone rhythmite cap carbonate is more organic-rich, while the upper is organic-poor, contains micritic limestone or dolomicrite ribbons and tubestone stromatolites at its base, and is known to contain limestone seafloor cements very similar in position and character to those in the Maieberg Formation. Both examples also record significant negative carbon isotope anomalies, with the upper event spanning a stratigraphic interval of hundreds of meters into the overlying Nama Group. These lithologic and geochemical similarities have been the basis for the direct correlation of the glacial deposits on the Congo and Kalahari cratons (Halverson et al., 2005). However, the strontium isotope composition of the limestone rhythmites, and seafloor precipitates interpreted as neomorphosed aragonite crystals, in the post-Blazkranz carbonates is significantly different, with lowest values near 0.7081 (Kaufman et al., 1997a,b; Misi et al., in press). The significant contrast between the $^{87}Sr/^{86}Sr$ composition of high Sr seafloor cements in the Maieberg (0.7073) and Tsabisis (0.7081) suggests that these are not correlative units.

Although none of the basal Lapa dolomicrites are a textural match for the cap carbonates on the Congo or Kalahari cratons, strontium isotope compositions may still be used to suggest a correlation. Unfortunately, all of the argillaceous Lapa samples are dolomite and most analyzed for $^{87}Sr/^{86}Sr$ composition are highly radiogenic. However, a single sample from micro-drilled micritic carbonates in shallow intertidal sediments from the KVD-F60 drillcore recorded a low value of ∼0.7068 (Azmy et al., 2001). A recent test of material from the same sample also yielded the same low $^{87}Sr/^{86}Sr$ result (Appendix A). Except for this least radiogenic value, it seems that the $^{87}Sr/^{86}Sr$ values of Lapa carbonates are significantly overprinted. Nonetheless, the lowest strontium isotope composition matches that found in the Rasthof Formation in Namibia, which is also consistent with the relative organic carbon contents of these rocks and the stratigraphic throw of the carbon isotope anomaly. This value does not match with limestone samples (including precipitates) from either the nearby Bambuí Group in Brazil, or from the Maieberg Formation in the Otavi Group in Namibia.

As an additional possible correlation tool, we analyzed trace sulfate in the Lapa carbonates for sulfur isotope compositions. Due to the general lack of bedded sulfates in this part of the stratigraphic column, little is known of secular changes in seawater sulfur isotope compositions. Such trends must therefore be regarded as a coarse tool at best given the lack of radiometric constraints and actual analyses, although remarkable variations in $\delta^{34}S$ through the Neoproterozoic and into the Cambrian Period have been documented—ranging from near +15‰ around 750 Ma to as high as +30‰ by the end of the Cambrian (Claypool et al., 1980; Strauss, 1993, 1997; Walter et al., 2000; Azmy et al., 2001; Strauss et al., 2001; Schröder et al., 2004; Goldberg et al., 2005).

Seawater SO_4^{2-} may be precipitated as evaporites (Thode and Monster, 1965; Claypool et al., 1980; Strauss, 1997) but their isotopic signature may reflect the influence of restricted local environment (closed basins) rather than open water. An alternative approach of obtaining more representative seawater $\delta^{34}S$ has been suggested by Strauss (1997 and references therein) by using the structurally substituted carbonate-associated sulfate (often referred to as CAS) that occur as trace constituent in the calcite lattice. Such analyses hold the ultimate promise of creating a high resolution sulfur isotope curve for the Neoproterozoic, but to date the focus of this technique has been on the post-glacial cap carbonates. CAS analyses of cap carbonates in Brazil (Kaufman et al., 2002) and Namibia (Hurtgen et al., 2002, 2005) reveal remarkable enrichments in ^{34}S (for example, up to ca. +45‰ in the Bambuí and Maieberg formations; the Rasthof Formation is similarly enriched, but to a lesser degree). The $\delta^{34}S$ values CAS in Lapa carbonates range from +12.2 to +24.3‰ (Appendix A). While some of these samples are enriched in ^{34}S against the Neoproterozoic background (similar to the cap carbonates discussed above), the high siliciclastic component of these sediments makes the interpretation of the values problematic.

6. Conclusion

Field, petrographic, and geochemical investigations of samples from several well preserved drillcores through the Lapa Formation reveal evidence for previously unrecognized glacial and post-glacial processes. Based on the sequence architecture, as well as lithologic succession and a strong regional negative carbon isotope anomaly, the basal Lapa Formation is considered as a cap carbonate lithofacies. Correlation of these beds with Neoproterozoic ice age deposits on the Congo and Kalahari cratons based on integrated stratigraphies, including a key strontium isotope result, suggests a direct equivalence with the Rasthof Formation in Namibia. This unit and the underlying Chuos diamictite are demonstrated to be younger than a 748 Ma ash layer beneath the glacial deposits. If correct, the basal Lapa Formation would most-likely be associated with the widespread Sturtian glacial episode.

The occurrence of an earlier glaciogenic unit (D) at the base of the Vazante Group (top of the St. Antônio do Bonito Formation) suggests a possible discrete earlier Sturtian glacial event (cf. Jacobsen and Kaufman, 1999, their Fig. 5; Halverson et al., 2005) or a pre-Sturtian glaciation. Both cases would still imply that the upper diamictites (DII) at the base of Lapa sequence be likely correlated with the Sturtian glaciation. Additional geochronological studies on the Vazante sequence will certainly provide more constraints on the age of the St. Antônio glaciation.

A second negative carbon isotope excursion is recognized in the upper part of the Lapa Formation. While this might correspond to a second Lapa ice age, the absence of diamictite at this level suggests that some other oceanographic process could be responsible. Further research into the age of the Lapa Formation is warranted, especially given the presence of organic-rich shale at its base. These post-glacial shales are the focus of new studies of biomarker assemblages and Re–Os radiometric determinations, which should shed important light on the timing and biotic response to Neoproterozoic ice age processes.

Acknowledgements

The authors wish to thank Dr. C. Calver, Prof. J. Veizer, and an anonymous reviewer for their constructive reviews and Votorantim Metais (Vazante, Minas Gerais, Brazil) for providing field assistance. This project was financed by Memorial University of Newfoundland (Canada), Pan-Atlantic Petroleum Systems Consortium (PPSC), Freiwillge Akademische Gesellschaft (FAG, Switzerland), and the Conselho Nacional de Desenvolvimento Científico e Tecnológico (CNPq, the National Research Council of Brazil). A.J.K. is supported by NSF grants EAR 040709 and 040113 and NASA Exobiology grant 040806-8733.

Appendix A

Samples, description, localities, stratigraphy, isotopic composition ($\delta^{18}O$ and $\delta^{13}C$ in ‰ VPDB and $\delta^{34}S$ in ‰ CDT), and trace element contents of the studied Lapa carbonates

Core	Sample ID	Depth (m)	Ca %	Mg %	Mn (ppm)	Sr (ppm)	Mn/Sr	Carbonate %	$\delta^{18}O$ VPDB	$\delta^{13}C$ VPDB	$^{87}Sr/^{86}Sr$	± 2σ	$\delta^{34}S$	$\delta^{13}C_{organic}$ VPDB	TOC %
MASOW 01	MAS 01	54.90	7.62	5.23	232	34	7	43	-7.63	-0.33				-15.8	0.025
	MAS 02	66.30							-7.56	-0.76					
	MAS 03	80.40							-7.12	-0.48					
	MAS 04	90.40							-6.86	-0.61					
	MAS 05	100.00							-7.86	-0.30					
	MAS 06	109.80	14.16	8.81	255	104	2	80	-7.11	0.49				-13.8	0.026
	MAS 07	135.50	16.33	9.70	587	93	6	79	-7.80	-1.07					
	MAS 08	148.90						58	-9.77	-1.92				-16.7	0.043
	MAS 09	158.60	6.42	3.65	2039	208	10	43	-10.49	-2.49					
	MAS 10	168.00	5.28	3.35	411	140	3	44	-10.95	-4.25				-21.5	0.032
	MAS 11	179.15	4.16	2.32	207	84	2	50	-10.83	-3.30			15.7		
	MAS 12	265.00	2.69	1.81	304	65	5	49	-10.13	-4.26				-14.2	0.014
	MAS 13	276.25						69	-7.74	0.04				-15.0	0.053
	MAS 15	288.60							-8.68	0.12	0.716639	0.000010			
	MAS 16	299.70	9.24	3.34	319	81	4	39	-8.52	0.29					
	MAS 17	316.00							-8.36	0.14					
	MAS 18	326.85							-8.31	0.15			24.3		
	MAS 19	339.65							-9.60	-0.24					
	MAS 20	353.85							-9.32	-0.74					
	MAS 21	363.50	7.32	4.09	497	69	7	50	-9.69	-0.19				-23.4	0.018
	MAS 22	373.15							-9.34	-0.14					
	MAS 23	384.35							-10.20	-0.84				-26.5	0.006
	MAS 25	405.80	11.12	2.80	578	141	4	30	-10.16	-0.66				-23.9	0.011
	MAS 26	415.75							-10.60	-0.84					
	MAS 27	425.00							-10.43	-0.66				-25.0	0.005
	MAS 28	435.65							-11.60	-1.32					
	MAS 29	446.15							-10.82	-0.62					
	MAS 30	456.90							-11.09	-1.02					
	MAS 31	467.30	3.80	2.40	396	48	8	23	-10.59	-0.71					
	MAS 32	474.00							-10.28	-0.77			18.1		
	MAS 33	480.40							-10.13	-0.72					
	MAS 34	489.40							-10.25	-0.81					
	MAS 35	496.10							-10.86	-1.18					
	MAS 36	505.00	13.57	8.20	931	156	6	52	-9.88	-0.75					
	MAS 37	515.10							-9.72	-0.38					
	MAS 38	523.85							-9.68	-0.82					
	MAS 39	531.00							-9.74	-0.95					
	MAS 40	539.25						45	-9.54	-1.04				-22.6	0.057
	MAS 41	547.25							-9.07	-0.67					
	MAS 42	554.80							-8.86	0.02					
	MAS 43	562.00							-9.24	-0.31					
	MAS 44	570.15	13.56	7.86	691	74	9	53	-8.07	0.11					
	MAS 45	579.10							-8.44	-0.33					
	MAS 46	589.35							-7.95	0.03					
	MAS 47	599.10						56	-8.99	-1.35			19.9	-24.8	0.010

Core	Sample ID	Depth (m)	Ca %	Mg %	Mn (ppm)	Sr (ppm)	Mn/Sr	Carbonate %	$\delta^{18}O$ VPDB	$\delta^{13}C$ VPDB	$^{87}Sr/^{86}Sr$	± 2σ	$\delta^{34}S$	$\delta^{13}C_{organic}$ VPDB	TOC %
	MAS 48	607.35							-9.15	-0.80					
	MAS 49	614.50	17.19	10.23	494	78	6	69	-7.33	-0.07					
	MAS 50	621.00							-8.09	-0.24					
	MAS 51	628.90						67	-7.67	0.11				-19.3	0.011
	MAS 52	636.15							-8.75	-0.26					
	MAS 53	645.40	14.31	9.11	637	87	7		-8.02	0.07					
	MAS 54	652.90							-6.55	0.12					
	MAS 55	658.50	19.37	12.11	688	102	7		-7.04	0.11			10.5		
	MAS 56	663.40							-8.42	-0.13					
	MAS 57	670.90						35	-7.16	0.04					
	MAS 58	680.55						65	-7.00	0.01				-18.5	0.008
	MAS 59	689.20							-6.54	0.39					
	MAS 60	696.00	26.43	16.78	532	98	5	61	-7.35	0.69					
	MAS 61	703.15							-5.91	0.48					
	MAS 62	706.30							-5.61	0.45					
	MAS 63	716.90							-5.37	0.31					
	MAS 64	724.85							-6.53	0.00					
	MAS 65	730.40							-5.98	0.01					
	MAS 66	735.00							-5.88	0.44					
	MAS 67	738.20	16.10	10.11	498	55	9	81	-5.67	1.01					
	MAS 68	740.00							-5.50	0.89					
	MAS 69	744.90							-5.89	0.94					
	MAS 70	748.10						68	-6.17	0.67				-15.1	0.018
	MAS 71	755.00	13.11	8.36	383	43	9	74	-6.13	0.18					
	MAS 72	758.70							-5.70	-0.41					
	MAS 73	760.25						69	-5.81	-0.30				-16.4	0.011
	MAS 74	767.00						66	-6.91	-2.54			22.7		
	MAS 75	777.20							-5.84	-0.56					
	MAS 76	781.80						77	-5.61	-0.27			13.8	-16.5	0.014
	MAS 77	792.10	1.70	0.63	278	27	10	46	-9.22	-2.85					
	MAS 78	797.35						48	-10.86	-5.47					
	MAS 79	823.70						54	-10.47	-4.32					
	MAS 80	827.60	6.33	2.39	1143	102	11	46	-10.57	-5.45				-23.7	0.056
	MAS 81	836.40							-9.13	-3.62			17.7		
	MAS 82	838.95							-10.08	-4.29					
	MAS 83	842.05							-8.96	-3.79					
	MAS 86	848.70	9.69	5.43	646	170	4	52	-8.90	-3.38				-23.4	0.004
	MAS 87	865.15							-9.35	-8.18			19.8		
	MAS 92	954.50	34.88	0.00	754	143	5	33	-8.51	1.68			12.6		
	MAS 96	1002.60							-7.09	1.36					
	MAS 59 E	689.20							-6.60	2.47					
	MAS 64 L	724.85							-8.40	1.12					
	MAS 64 F	724.85							-10.05	-4.08					
	MAS 66 L	735.00							-9.89	-4.48					
	MAS 66 E	735.00							-6.26	0.84					
	MAS 69 L	744.90							-6.97	0.09					

Core	Sample ID	Depth (m)	Ca %	Mg %	Mn (ppm)	Sr (ppm)	Mn/Sr	Carbonate %	δ^{18}O VPDB	δ^{13}C VPDB	^{87}Sr/^{86}Sr	± 2σ	δ^{34}S	$\delta^{13}C_{organic}$ VPDB	TOC %
	MAS 79 L	823.70							-6.93	0.18					
	MAS 82 L	838.95							-6.87	-0.57					
	MAS 92 L	954.50							-6.97	-0.44					
	MAS 92 E	954.50							-7.44	0.08					
MAF 38-84	F 01	501.30							-9.37	-0.80					
	F 03	508.05							-9.29	-0.42					
	F 04	511.05											12.8		
	F 06	517.40							-9.06	-0.30					
	F 09	527.15							-9.90	-0.49					
	F 11	535.00							-9.59	-0.24					
	F 13	542.00							-10.08	-0.51			12.2		
	F 14	545.10							-9.73	-0.47					
	F 15	548.30							-9.53	-0.45					
	F 16	552.20							-9.45	-0.38					
	F 17	555.10							-9.68	-0.62					
	F 19	561.00	11.45	5.62	826	134	6		-8.97	-0.21					
	F 20	564.80							-8.80	-0.27					
	F 21	567.75							-8.77	-0.44					
	F 22	570.75							-8.67	-0.34					
	F 23	574.95	6.73	0.81	97	11	9		-8.34	-0.78			14.1		
	F 24	578.15							-8.00	-0.08					
	F 25	581.25							-8.13	-0.24					
	F 26	584.30							-8.21	0.07					
	F 27	588.44	11.18	5.44	484	47	10		-8.26	0.27					
	F 28	592.20							-7.93	0.23			16.1		
	F 29	596.60							-7.89	0.17					
	F 30	599.50							-7.65	0.00					
	F 31	605.70							-7.22	0.06					
	F 32	609.50							-7.43	0.32					
	F 33	613.00							-6.87	-0.03					
	F 34	617.00							-6.74	-0.28					
	F 35	619.15							-5.75	-0.23					
	F 36	621.50							-5.22	0.00					
	F 37	625.20	13.38	8.58	255	71	4		-4.95	0.88	0.722916	0.000010			
	F 38	628.30							-5.83	0.00					
	F 39	632.60							-5.09	-0.14			14.8		
	F 40	636.00							-5.55	-0.05					
	F 41	639.70							-5.56	-0.16					
	F 42	644.25	15.53	8.90	658	95	7		-6.66	0.71					
	F 43	648.40							-5.96	0.42					
	F 44	651.80	13.76	8.29	386	49	8		-4.91	-2.65			23.2		
	F 45	655.00							-5.42	-0.75					
	F 46	661.00							-5.86	-0.18					
	F 13 L	542.00							-9.08	-1.00					
	F 14 L	545.10							-9.60	-1.54					

Appendix A (*Continued*)

Core	Sample ID	Depth (m)	Ca %	Mg %	Mn (ppm)	Sr (ppm)	Mn/Sr	Carbonate %	$\delta^{18}O$ VPDB	$\delta^{13}C$ VPDB	$^{87}Sr/^{86}Sr$	± 2σ	$\delta^{34}S$	$\delta^{13}C_{organic}$ VPDB	TOC %
	F 29 L	596.60							-1.12	-1.20					
PMA 04	A 01	111.50	25.11	1.52	826	418	2		-12.09	-2.26			16.5		
	A 02	124.90	26.16	0.69	2373	369	6		-12.48	-3.53					
	A 03	150.15	8.09	2.15	781	54	15		-10.95	-3.47					
	A 04	171.70	30.17	0.95	2577	496	5		-11.98	-3.40	0.723845	0.000015			
	A 05	200.80							-10.08	-1.34					
	A 06	274.65							-8.07	-0.20					
	A 07	296.00							-7.36	0.06					
	A 08	333.00	11.22	6.64	564	43	13		-5.81	0.60			13.1		
	A 09	358.00							-6.29	-0.52					
	A 10	360.00							-8.00	-1.04					
	A 11	362.70							-8.56	-0.51					
	A 12	365.00							-6.39	-0.86					
	A 13	368.30							-6.99	-1.96					
	A 14	372.00							-6.12	-1.80					
	A 15	375.70							-5.67	-1.75					
	A 17	381.00							-7.01	-2.25	0.747388	0.000010			
	A 19	384.50							-6.16	-2.46	0.752196	0.000010			
	A 21	386.90							-6.17	-1.65					
	A 22	390.70							-5.03	0.43			12.7		
	A 24	392.90							-6.55	-0.34					
	A 25	397.00							-6.13	0.14					
	A 26	402.00							-6.09	-0.79					
	A 27	403.30							-6.43	-0.35			16.4		
	A 28	406.40							-5.26	0.57					
	A 29	409.70							-5.53	0.59					
	A 13 L	368.30							-8.18	-2.32					
	A 22 F	390.70							-7.24	-1.77					
KVD-F60	KV60-01	284			36	314	0		-12.3	-2.9	0.717515	0.000006	22.0		
	KV60-03	310			37	570	0		-9.7	-1.8	0.706841	0.000008	18.0		
	KV60-03b	310									0.706901	0.000007			
	KV60-04	416			2791	852	3		-12.8	-2.1	0.730735	0.000009			
	KV60-04b	496							-3.4	2.3					
	KV60-05	539							-3.79	0.78					
	KV60-06	539			273	92	3		-3.79	0.78					
	KV60-06b	550							-2.17	2.21					
	KV60-07	557							-3.15	1.50					
	KV60-07a	562							-2.13	1.89					
	KV60-07b	568							-0.86	2.37					
	KV60-08	586							-2.48	2.51					
	KV60-09	573							-1.26	2.58			12.4		
	KV60-10	93			1621	127	13		-7.7	-0.4	0.724166	0.000008	21.0		
	KV60-11	204							-13.56	1.05					
	KV60-12	244			1130	87	13		-7.0	0.5	0.716869	0.000009			

Appendix A (*Continued*)

Core	Sample ID	Depth (m)	Ca %	Mg %	Mn (ppm)	Sr (ppm)	Mn/Sr	Carbonate %	δ^{18}O VPDB	δ^{13}C VPDB	$^{87}Sr/^{86}Sr$	± 2σ	δ^{34}S	$\delta^{13}C_{organic}$ VPDB	TOC %
	KV60-13	212							-11.50	0.68					
	KV60-15	525			153	47	3		-4.2	2.9					
	KV60-15a	531							-1.77	3.32					
	KV60-15b	535							-2.17	2.74					
	KV60-16	577			47	50	1		-1.04	2.68					
	KV60-17	613							-2.48	2.39					
	KV60-5 F	496							-5.4	2.2					
	KV60-8 F	586									0.710058	0.000008			
	KV60-12 L	244							-9.0	-0.5					
	KV60-15 L	525							-9.8	2.3					
	KV60-16 F	577									0.710463	0.000008			

F = fibrous cement, E = early equant cement, L = late fracture filling cement.

Highlighted samples from Azmy et al. (2001). F, fibrous cement; E, early equant cement; L, late fracture filling cement.

References

Alkmim, F.F., Brito Neves, B.B., Alves, J.A.C., 1993. Arcabouço tectônico do Craton do São Francisco, Uma revisão. In: Dominguez, J.M.L., Misi, A. (Eds.), O Craton do São Francisco, SBG BA–SE/SGM/CNPq, Salvador, BA, Brasil, pp. 45–62.

Azmy, K., Veizer, J., Wenzel, B., Bassett, M.G., Copper, P., 1999. Silurian strontium isotope stratigraphy. GSA Bull. 111, 475–483.

Azmy, K., Veizer, J., Misi, R., De Olivia, T., Dardenne, M., 2001. Isotope stratigraphy of the neoproterozoic carbonate of vazante formation Saõ Francisco Basin, Brazil. Precambrian Res. 112, 303–329.

Banner, J.L., Hanson, G.N., 1990. Calculations of simultaneous isotopic and trace element variations during water-rock interaction with applications to carbonate diagenesis. Geochim. Cosmochim. Acta 54, 3123–3137.

Bowring, S., Myrow, P., Landing, E., Ramezani, J., Grotzinger, J., 2003. Geochronological constraints on terminal Proterozoic events and the rise of metazoans. Geophys. Res. Abstr. 5, 219 (EGS, Nice).

Brand, U., Veizer, J., 1980. Chemical diagenesis of a multicomponent carbonate system: 1. Trace elements. J. Sediment. Petrol. 50, 1219–1236.

Brasier, M.D., Shields, G.A., 2000. Chemostratigraphy and correlation of the Neoproterozoic Port Askaig glaciation, Dalradian Supergroup of Scotland. J. Geol. Soc. (Lond.) 157, 909–914.

Brody, K.B., Kaufman, A.J., Eigenbrode, J., Cody, J., 2004. Biomarker geochemistry of a post-glacial Neoproterozoic succession in Brazil. In: Geological Society of America Annual Meeting, Denver, CO, 7–10 November 2004 (Abstract).

Burdett, J.W., Grotzinger, J.P., Arthur, M.A., 1990. Did major changes in the stable-isotope composition of Proterozoic seawater occur? Geology 18, 227–230.

Calver, C.R., 2000. Isotope stratigraphy of the Ediacarian (Neoproterozoic III) of the Adelaide Rift Complex, Australia, and the overprint of water column stratification. Precambrian Res. 100, 121–150.

Campos-Neto, M.C., 1984. Litoestratigrafia, relações estratigráficas e evolução paleogeográfica dos grupos Canastra e Paranoá (região Vazante-Lagamar, MG). Revista Brasileira de Geociências 14, 81–91.

Chemale F.Jr., Alkmim, F.F., Endo, I., 1993. Late Proterozoic tectonism in the interior of the Saõ Francisco craton. In: Findlay, R.H., Unrug, R., Banks, M.R., Veever, J.J. (Eds.), Gondwana Assembly—Assembly, Evolution and Dispersal. Balkema, Rotterdam, pp. 29–42.

Claypool, G.E., Holser, W.T., Kaplan, I.R., Sakai, H., Zak, I., 1980. The age curves of sulfur and oxygen isotopes in marine sulfate and their mutual interpretation. Chem. Geol. 28, 199–260.

Cloud, P.E., Dardenne, M.A., 1973. Proterozoic age of the Bambuí Group in Brazil. GSA Bull. 84, 1673–1676.

Coleman, M.L., Walsh, J.N., Benmore, R.A., 1989. Determination of both chemical and stable isotope composition in milligram-size carbonate samples. Sediment. Geol. 65, 233–238.

Condon, D., Zhu, M., Bowring, S., Wang, W., Yang, A., Jin, Y., 2005. U–Pb ages from the Neoproterozoic Doushantuo formation. Chin. Sci. 308, 95–97.

Corsetti, F.A., Kaufman, A.J., 2003. Stratigraphic investigations of carbon isotope anomalies and Neoproterozoic ice ages in Death Valley. CA Geol. Soc. Am. Bull. 115, 916–932.

Cozzi, A., Allen, P., Grotzinger, J., 2004. Understanding carbonate ramp dynamics using δ^{13}C profiles: examples from the Neoproterozoic Buah Formation of Oman. Terra Nova 16, 62–67.

Dardenne, M.A., 1978. Sentese sobre a estratigrafiado Groupo Bambuí no Brasil Central. Trigésimo Congresso Brasileiro de Geologia 2, 597–610.

Dardenne, M.A., 2000. The Brasilia Fold Belt. In: Cordani, U.G., Milani, E.J., Thomaz-Filho, A., Campos, D.A. (Eds.), Tectonic Evolution of South América. 31st International Geological Congress. Rio de Janeiro, pp. 231–263.

Dardenne, M.A., 2001. Lithostratigraphic sedimentary sequences of the Vazante Group. IGCP 450 Proterozoic sediment-hosted base metal deposits of western Gondwana (Abstr.), Belo Horizonte, Brazil, p. 48–50.

Dardenne, M.A., Walde, D.H.G., 1979. A estratigrafia dos Grupos Bambuí e Macaúbas no Brasil Central. Bol. Soc. Bras. Geol., Núcleo Minas Gerais 1, 43–53.

D'Agrella-Fihlo, M.S., Babinski, M., Trindade, R.I.F., Van Schmus, W.R., Ernesto, M., 2000. Simultaneous remagnetization and U-Pb isotope resin Neoproterozoic carbonates of the São Francisco craton, Brazil. Precambrian Res. 99, 179–196.

Derry, L.A., Kaufman, A.J., Jacobsen, S.B., 1992. Sedimentary cycles and environmental change in the Late Proterozoic: evidence from stable and radiogenic isotopes. Geochim. Cosmochim. Acta 56, 1317–1329.

Dickson, J.A.D., 1966. Carbonate identification and genesis as revealed by staining. J. Sed. Petrol. 36, 491–505.

Diener, A., Ebneth, S., Veizer, J., Buhl, D., 1996. Strontium isotope stratigraphy of the Middle Devonian: brachiopods and conodonts. Geochim. Cosmochim. Acta 60, 639–652.

Fairchild, I.J., Spiro, B., 1987. Petrological and isotopic implications of some contrasting Late Precambrian carbonates, NE Spitsbergen. Sedimentology 34, 973–989.

Fairchild, T.R., Schopf, J.W., Shen-Miller, J., Guimarães, E.M., Edwards, M.D., Lagstein, A., Li, X., Pabst, M., De Melo-Filho, L.S., 1996. Recent discoveries of Proterozoic microfossils in south-central Brazil. Precambrian Res. 80, 125–152.

Fuck, R.A., Pimentel, M.M., Silva, J.H.D., 1994. Compartimentação tectônica na porção oriental da Província Tocantins. 38° Congresso Brasileiro de Geologia, Camboriú—Sociedade Brasileira de Geologia. Anais 1, 215–216.

Goldberg, T., Poulton, S.W., Strauss, H., 2005. Sulphur and oxygen isotope signatures of late Neoproterozoic to early Cambrian sulphate, Yangtze Platform, China: diagenetic constraints and seawater evolution. Precambrian Res. 137, 223–241.

Hall, G.E.M., Pelchat, J.-C., Loop, J., 1988. Separation and recovery of various sulphur species in sedimentary rocks for stable sulphur isotopic determination. Chem. Geol. 67, 35–45.

Halverson, G.P., Hoffman, P.F., Schrag, D.P., Maloof, A.C., Rice, A.H.N., 2005. Toward a Neoproterozoic composite carbon-isotope record. Geol. Soc. Am. Bull. 117, 1181–1207.

Hayes, J.M., Kaplan, I.R., Wedeking, K.W., 1983. Precambrian organic geochemistry; preservation of the record. In: Schopf, J. (Ed.), Earth's Earliest Biosphere: Its Origin and Evolution. Princeton University Press, Princeton, NJ, United States, pp. 93–134.

Hoffman, P.F., Hawkins, D.P., Isachsen, C.E., Bowring, S.A., 1996. Precise U-Pb zircon ages for early Damaran magmatism in the Summas Mountains and Welwitschia Inlier, northern Damara belt, vol. 11. Communications of the Geological Survey of Namibia, Namibia, pp. 47–52.

Hoffman, P.F., Kaufman, A.J., Halverson, G.P., Schrag, D.P., 1998a. A Neoproterozoic snowball Earth. Science 281, 1342–1346.

Hoffman, P.F., Kaufman, A.J., Halverson, G.P., 1998b. Comings and goings of global glaciation on a Neoproterozoic tropical platform in Namibia. GSA Today 8, 1–9.

Hurtgen, M.T., Arthur, M.A., Halverson, G.P., 2005. Neoproterozoic sulfur isotopes, the evolution of microbial sulfur species, and the burial efficiency of sulfide as sedimentary pyrite. Geology 33 (1), 41–44.

Hurtgen, M.T., Arthur, M.A., Suits, N.S., Kaufman, A.J., 2002. The sulfur isotopic composition of Neoproterozoic seawater sulfate: implications for a snowball earth? Earth Planet. Sci. Lett. 203, 413–430.

Jacobsen, S.B., Kaufman, A.J., 1999. The Sr, C and O isotope evolution of Neoproterozoic seawater. Chem. Geol. 161, 37–57.

Karfunkel, J., Hoppe, A., 1988. Late Proterozoic glaciation in central-eastern Brazil: synthesis and model. Paleogeogr. Paleoclimat. Plaeoecol. 65, 1–21.

Kaufman, A.J., Corsetti, F.A., Varni, M.A. The effect of rising atmospheric oxygen on carbon and sulfur isotope anomalies in the Neoproterozoic Johnnie Formation, Death Valley. Chem. Geol., in press (special issue).

Kaufman, A.J., Hayes, J.M., Knoll, A.H., Germs, G.J.B., 1991. Isotopic compositions of carbonates and organic carbon from upper Proterozoic successions in Namibia: stratigraphic variation and the effect of diagenesis and metamorphism. Precambrian Res. 49, 301–327.

Kaufman, A.J., Hoffman, P.F., Halverson, G.P., 1997a. Comings and goings of Neoproterozoic ice ages in Namibia. In: Annual Meeting, Geological Society of America, vol. 29(6), p. 196 (Abstracts).

Kaufman, A.J., Jacobsen, S.B., Knoll, A.H., 1993. The Vendian record of Sr- and C-isotopic variations in seawater: implications for tectonics and paleoclimate. Earth Planet. Sci. Lett. 120, 409–430.

Kaufman, A.J., Knoll, A.H., 1995. Neoproterozic variations in the C-isotopic composition of seawater: stratigraphic and biogeochemical implications. Precambrian Res. 73, 27–49.

Kaufman, A.J., Knoll, A.H., Awramik, S.M., 1992. Biostratigraphic and chemostratigraphic correlation of Neoproterozoic sedimentary successions: Upper Tindir Group, northwestern Canada, as a test case. Geology 20, 181–185.

Kaufman, A.J., Knoll, A.H., Narbonne, G.M., 1997b. Isotopes, ice ages and terminal Proterozoic Earth history. Proc. Natl. Acad. Sci. 94, 6600–6605.

Kaufman, A.J., Varni, M.A., Wing, B., 2002. Sulfur isotope constraints on the snowball Earth. Geol. Soc. Am. 34, 221 (Abstracts with programs).

Kendall, B.S., Creaser, R.A., Ross, G.M., Selby, D., 2004. Constraints on the timing of Marinoan "Snowball Earth" glaciation by ^{187}Re-^{187}Os dating of a Neoproterozoic, post-glacial black shale in Western Canada. Earth Planet. Sci. Lett. 222, 729–740.

Kirschvink, J.L., 1992. Late Proterozoic lowlatitude glaciation: The snowball Earth. In: Schopf, J.W., Klein, C. (Eds.), The Proterozoic Biosphere: A Multidisciplinary Study. Cambridge University Press, Cambridge, pp. 51–52.

Knoll, A.H., Hayes, J.M., Kaufman, A.J., Swett, K., Lambert, I.B., 1986. Secular variations in carbon isotope ratios from Upper Proterozoic successions of Svalbard and East Greenland. Nature 321, 832–838.

Lagoeiro, L.E., 1990. Estudo da deformação nas sequências carbonáticas do Grupo Una na região de Irecê. BA M.Sc. Dissertation, Universidade Federal de Ouro Preto, Brazil.

Machel, H.G., Burton, E.A., 1991. Factors governing cathodoluminescence in calcite and doloomite, and their implications for studies of carbonate diagenesis. In: Luminescence Microscopy, Spectroscopy, Qualitative, Quantitative Applications, SEPM. Short Course, vol. 25, pp. 37–57.

Madalosso, A., 1979. Stratigraphy and sedimentation of the Bambuí Group in Paracatu region, Minas Gerais. Brazil. MSc. Thesis, University of Missouri, 127 pp.

Misi, A., 2001. Estratigrafia isotópica das seqüências do Supergrupo São Francisco coberturas neoproterozócias do craton do São Francisco. Idade e correlacoes. In: C.P. Pinto, M.A. Martins-Neoto, (Eds.), Bacia do São Francisco. Geologia e Recursos Naturais. SBG, Nucoe de Minas Gerais, pp. 67–92.

Misi, A., Iyer, S.S., Coelhoa, C.E., Tassinarie, C.C., Franca-Rochaa, W.J., Cunhab, I., Gomes, A.S., de Oliveira, T.F., Teixeira, J.B., Filho, V.M., 2005. Sediment hosted lead–zinc deposits of the Neoproterozoic Bambuí Group and correlative sequences, São Francisco Craton, Brazil: A review and a possible metallogenic evolution model. Ore Geol. Rev. 26, 263–304.

Misi, A., Kaufman, A.J., Veizer, J., Powis, K., Azmy, K., Boggiani, P.C., Gaucher, C., Teixeira, J.B.G., Sanches, A.L., Iyer, S.S. Chemostratigraphic correlation of Neoproterozoic successions in South America. Chem. Geol., in press.

Misi, A., Veizer, J., 1998. Neoproterozoic carbonate sequences of the Una Group, Irecê Basin, Brazil: chemostratigraphy, age and correlations. Precambrian Res. 89, 87–100.

Narbonne, G.M., Kaufman, A.J., Knoll, A.H., 1994. Integrated chemostratigraphy and biostratigraphy of the Windermere Supergroup, northern Canada: implications for Neoproterozoic correlations and early evolution of animals. GSA Bull. 106, 1281–1292.

Olcott, A.N., Sessions, A.L., Corsetti, F.A., Kaufman, A.J., de Oliviera, T.F., 2005. Biomarker evidence for photosynthesis during Neoproterozoic glaciation. Science 310, 471–474.

Rush, P.F., Chafetz, H.S., 1990. Fabric retentive, non-luminescent brachiopods as indicators of original δ^{13}C and δ^{18}O compositions: a test. J. Sediment. Petrol. 60, 968–981.

Saylor, B.Z., Kaufman, A.J., Grotzinger, J.P., Urban, F., 1998. A composite reference section for terminal Proterozoic strata of southern Namibia. J. Sedimentary Res. 68, 1223–1235.

Schröder, S., Schreiber, B.C., Amthor, J., Matter, A., 2004. Stratigraphy and environmental conditions of the terminal Neoproterozoic–Cambrian Period in Oman: evidence from sulphur isotopes. J. Geol. Soc. Lond. 161, 489–499.

Shields, G.A., Stille, P., Brasier, M.D., Atudorei, V., 1998. Ocean stratification and oxygenation of the Late Precambrian environment: a post-glacial geochemical record from a Neoproterozoic section in W. Mongolia. Terra Nova 9, 218–222.

Shields, G.A., Veizer, J., 2002. Precambrian marine carbonate isotope database: Version 1.1. Geochem. Geophys. Geosyst. vol. 3 (6), 1031, doi:10.1029/2001GC000266.

Strauss, H., 1993. The sulfur isotopic record of Precambrian sulfates: new data and a critical evaluation of the existing record. Precambrian Res. 63, 225–246.

Strauss, H., 1997. The isotopic composition of sedimentary sulfur through time. Paleogeogr. Paleoclim. Paleoecol. 132, 97–118.

Strauss, H., Banerjee, D.M., Kumar, V., 2001. The sulfur isotopic composition of Neoproterozoic to early Cambrian seawater–evidence from the cyclic Hanseran evaporites, NW India. Chem. Geol. 175, 17–28.

Thode, H.G., Monster, J., 1965. Sulfur isotope geochemistry of petroleum, evaporites, and ancient seas. Am. Assoc. Pet. Geol. Mem. 4, 367–377.

Valeriano, C.M., Dardenne, M.A., Fonseca, M.A., Simões, L.S.A., Seere, H.J., 2004. A evolução tectônica da Faixa Brasília. In: Mantesso-Neto, V., Bartorelli, A., Carneiro, C.D.R., Neves, B.B. (Eds.), Geologia do Continente Sul Americano: Evolução da Obra de Fernando Flávio Marques de Almeida, Editora Beca, pp. 575–593.

Veizer, J., 1983. Chemical diagenesis of carbonates: theory and application of trace element technique. In: Arthur, M.A., Anderson, T.F., Kaplan, I.R., Veizer, J., Land, L.S. (Eds.), Stable Isotopes in Sedimentary Geology. Society of Economic Paleontologists and Mineralogists (SEPM) Short Course Notes, vol. 10, pp. III-1–III-100.

Veizer, J., Ala, D., Azmy, K., Bruckschen, P., Bruhn, F., Buhl, D., Carden, G., Diener, A., Ebneth, S., Goddris, Y., Jasper, T., Korte, C., Pawellek, F., Podlaha, O., Strauss, H., 1999. ^{87}Sr/^{86}Sr, δ^{18}O and δ^{13}C evolution of Phanerozoic seawater. Chem. Geol. 161, 59–88.

Walter, M.R., Veevers, J.J., Calver, C.R., Gorjan, P., Hill, A.C., 2000. Dating the 840–544 Ma Neoproterozoic interval by isotopes of strontium, carbon, and sulfur in seawater, and some interpretative models. Precambrian Res. 100, 371–433.

Yoshioka, H., Asahara, Y., Tojo, B., Kawakami, S., 2003. Systematic variations in C, O, and Sr isotopes and elemental concentrations in Neoproterozoic carbonates in Namibia: implications for a glacial to interglacial transition. Precambrian Res. 124, 69–85.